Optical Properties of Carbon Nanoparticles by Laser Ablation in Nonionic Surfactant Aqueous Solution

Taichi Okumura and Hiroyuki Wada*

School of Materials and Chemical Technology, Institute of Science Tokyo, 4259 Nagatsuta-cho, Midoriku-ku, Yokohama 226-8502 Japan
**Corresponding author's e-mail: wada.h.ac@m.titech.ac.jp*

Carbon nanoparticles (CNPs) were successfully prepared in pure water and nonionic surfactant aqueous solutions by a liquid laser ablation method. CNPs were obtained from micron-sized carbon black powder by laser irradiation (Nd:YAG, SHG) in a solvent. The prepared CNPs were evaluated by scanning electron microscopy, dynamic light scattering, UV-visible spectrophotometry, fluorescence spectrophotometry, Raman spectrophotometry, and Fourier transform infrared spectrophotometry. CNPs prepared by laser irradiation showed reduced secondary particle size compared to the raw materials, making them suitable for biomedical applications; CNPs exhibited blue and green fluorescence, and the blue to green fluorescence intensity ratio The D/G ratio of the CNPs increased slightly, suggesting the presence of MO-PEG on the particle surface. Therefore, the prepared CNPs are useful for establishing highly accurate bioimaging using dual fluorescence.
Keywords: carbon, nanoparticles, surfactant, laser process, dual fluorescence

DOI: 10.2961/jlmn.2025.02.2001

1. Introduction

Nanomaterials with excellent physical and chemical properties are dealt with in a wide range of fields such as science, engineering, and medicine, and are used in numerous products to support people's lives. Among them, nanomaterials called quantum dots are commonly known as nanoparticles with sizes smaller than the exciton Bohr radius [1], and their high photostability and long fluorescence lifetime have been investigated for applications in optical and electrical devices [2, 3]. Semiconductor quantum dots fabricated from conventional group II-VI and III-V semiconductors such as cadmium selenide CdSe and indium phosphide InP can reproduce various colors due to the quantum size effect, and exhibit upconversion emission by two-photon excitation, their application to bioimaging has been investigated [4, 5, 6]. However, heavy metals such as cadmium and selenium used in semiconductor quantum dots are known to cause acute and chronic toxicity in humans and other vertebrates [7, 8], and Peter H. M. Hoet et al. have demonstrated that surface carboxylated CdSe/ZnS core-shell quantum dots in mice and found that the surface carboxylated CdSe/ZnS core-shell quantum dots had a prothrombogenic effect [9]. In addition, indium and selenium are known as rare metals, and the issue of high production costs in countries with scarce reserves of these metals has been raised [10, 11].

Carbon quantum dots (CQDs) are the first carbon-based nanomaterials obtained by electrochemical processing of single-walled carbon nanotubes [12], and their unique structure and properties have led to their investigation for applications in chemical sensors [13], biosensors [14], photocatalysis [15], electrocatalysis [16]. CQDs have attracted much attention even now, more than 10 years after their first report [17, 18, 19] and are expected to be a promising alternative to semiconductor quantum dots due to their excellent optical properties, such as high quantum yield and excitation wavelength-dependent fluorescence. Compared to conventional semiconductor quantum dots, CQDs have superior biocompatibility and water solubility, which has led to active research on their application, especially in the biomedical field [20, 21]. Huang et al. studied the distribution of CQD in the body, the rate of its extracorporeal elimination, and the effect of injection site on the accumulation of CQD and found that intravenous injection resulted in the fastest CQD elimination [21].

The synthesis pathway of CQDs can be divided into two types: bottom-up and top-down methods. The bottom-up method obtains CQDs by thermal treatment of organic molecules such as citric acid and urea, and includes microwave [22], hydrothermal [23], and pyrolysis [23] methods. CQDs were prepared by dissolving citric acid monohydrate in water and hydrothermally treating it at 300°C for 2 hours in a stainless-steel autoclave [23]. The bottom-up method has also been reported to produce CQDs from familiar organic materials such as glucosamine [24], orange juice [25], and chicken eggs [26]. The preparation of CQDs by the bottom-up method often requires high temperature, high pressure, and long time for the reaction to proceed completely, plus post-treatment to extract unreacted components. On the other hand, the top-down method produces CQDs from carbon materials such as graphite and carbon nanotubes, and is fabricated by arc discharge [12], chemical oxidation [27], electrochemical methods [28], and pulsed laser ablation in liquid.

Pulsed laser ablation in liquid (PLAL) was first reported in 1987 by Ogale, Patil et al. to obtain nanoparticles by irradiating a metal target in liquid with a high-power Q-switched pulsed ruby laser [29, 30], and a tablet-like solid, called a target, immersed in a solvent The first report of nanoparticles obtained by irradiating a tablet-like solid called a target immersed in a solvent or in suspension is a physical method to obtain nanoparticles through the interaction between the laser and the material by irradiating the target with the laser

[31, 32]. (i) A portion of the laser pulse reaches the target surface, and the electrons are converted into plasma in the laser target, then producing a plasma plume composed of atoms, electrons, and ions. (ii) The continuous laser pulse causes the plasma plume to adiabatically expand, and a vapor layer is formed around the plasma plume by energy transfer to the surrounding liquid, resulting in the formation of cavitation bubbles. (iii) Repeated expansion and compression of the cavitation bubble causes rapid cooling and contraction of the plasma plume, resulting in the release of nanoparticles. PLAL has the advantages of controlling the size of nanoparticles by controlling parameters such as wavelength, pulse width, fluence, and irradiation time [33], fabrication at ambient temperature and pressure and in an oxygen atmosphere [33], and obtaining highly crystalline nanoparticles [33, 34]. In the first report on CQDs fabrication by PLAL, G.-W. Yang et al. successfully fabricated nanodiamonds by irradiating a polycrystalline graphite target in pure water with a 532 nm Nd:YAG laser for 30 min [35]. Since then, there have been many reports of fabrication from multi-walled carbon nanotubes [36], graphite [37], and carbon black [38].

In this study, CNPs with blue and green dual emission properties were prepared in a one-step process by PLAL using aqueous polyethylene glycol monooleate (MO-PEG), a nonionic surfactant registered as a quasi-drug additive in Japan[39], as a solvent and carbon black as a suspension. The CNPs were prepared by irradiating a suspension of carbon black with a non-focusing horizontal Nd:YAG laser. The CNPs produced were within the EPR effect range (10 nm < Φ < 200 nm), which is important for medical applications of nanoparticles, and were of a size that was not affected by in vitro discharge from the kidney (< 10 nm) or liver (> 500 nm) (EPR effect: phenomenon in which angiogenesis caused by cancer cell proliferation creates a space of 10-200 nm in the vessel wall; controlling the nanoparticles in this range allows them to selectively accumulate in cancer cells) [40, 41, 42]. In addition, CNPs showed differences in the intensity ratio of blue to green emission depending on the MO-PEG concentration. Although previous studies have involved acid treatment of nanoparticles after laser ablation [43] and laser ablation of carbon materials in organic solvents such as ethanol and acetone to produce CQDs with monochromatic emission [44, 45, 46], the process reported here is simpler in operation and a new fabrication method for CNPs that is biocompatible in that it is composed of materials that have little impact on the human body in addition to being simple to operate.

2. Experimental section

2.1 Materials

Carbon black (particle size < 100 nm) was purchased from Sigma-Aldrich Co. (USA) and polyethylene glycol monooleate (MO-PEG) from FUJIFILM Wako Pure Chemical Co. (Japan). Pure water was purified from Simplicity® UV by Merck Millipore. All reagents were used without purification.

2.2 Preparation of nanoparticles

4 mg of carbon black and solvent were placed in a square container (soda glass, transparent) and irradiated with a horizontal unfocused laser for 30 minutes. The laser was an Nd:YAG laser (Continuum, Powerlite 8010, wavelength 532 nm, pulse width 5-7 ns, repetition rate 10 Hz, fluence 600 mJ/cm^2). The solvents used were 20 mL each of pure water and 0.003, 0.006, and 0.012 vol% MO-PEG. The carbon black was irradiated by laser while stirring with a magnetic stirrer to prevent precipitation and agglomeration of carbon black. After laser irradiation, the product was filtered through a syringe filter (glass fiber, pore size 1 um, AZ ONE) to remove unreacted material.

2.3 Instruments and Characterizations

Particle shape and size were evaluated using a scanning electron microscope (SEM, Hitachi High-Tech Co., S-4800) and dynamic light scattering (DLS, Horiba, Ltd., nanoPartica SZ-100V2) SEM is a copper STEM grid coated with a 100 mesh carbon support film DLS was measured with 3 mL of sample solution in a 4-sided transmission plastic cell at a wavelength of 532 nm and a detector angle of 90°.

Optical properties were evaluated using a UV-Vis spectrophotometer (UV-Vis, JASCO Co., V-670) and a spectrofluorometer (PL, Hitachi High-Tech, F-7000). UV-vis spectra were measured in a 3 mL quartz cell with a dilution the sample solution of 10 times with pure water, 1 nm resolution, 2 nm band width, scanning speed For PL spectra, 3 mL of sample solution was placed directly in a quartz cell and measured at an excitation wavelength of 360 nm, a scanning speed of 240 nm/min, slits width on the excitation and fluorescence sides of 5 nm, and a PMT voltage of 400 V.

Composition and surface analysis were measured with a Raman microscope (Horiba, Ltd., XploRA PLUS) and a Fourier transform infrared spectrophotometer (FT-IR, SHIMADZU Co., IRPrestige-21). Raman spectra were measured by depositing solid samples obtained by freeze-drying nanoparticle-dispersed solution to remove solvent (TOKYO RIKAKIKAI CO., LTD., FDU-1200) for several days on glass slides at a wavelength of 532 nm, exposure time of 20 seconds, grating 600 gr/mm, integration frequency of 2 times, and attenuation filter of 10%. FT-IR was also measured by depositing samples after freeze-drying on prisms and Apodize function Happ-Genzel, 40 integration times, resolution 4 cm^{-1}.

3. Results and Discussion

SEM images of the nanoparticles resulting from laser irradiation of the raw material and carbon black suspension in pure water at different fluences are shown in Fig. 1, and their respective particle size distributions are shown in Fig. 2. The raw material consisted of aggregated spherical particles, with a primary particle size of 33 ± 9 nm and a secondary particle size of 5 ± 2 um (Fig.1 (a), Fig.2 (a)). After laser irradiation in pure water, spherical particles agglomerated as in the raw material, 75 mJ/cm^2: 40 ± 9 nm, 150 mJ/cm^2: 44 ± 9 nm, 300 mJ/cm^2: 33 ± 8 nm, 600 mJ/cm^2: 45 ± 10 nm (Fig.1. (b-e), Fig.2. (b-e)). The primary particle sizes, the dimensions of the smallest unit of particles, of the nanoparticles prepared in pure water were almost the same as those of raw materials.

SEM images of nanoparticles obtained by laser irradiation of carbon black suspensions in MO-PEG aqueous solutions of different concentrations with a laser fluence of 600 mJ/cm^2 are shown in Fig. 3 and their respective particle size distributions in Fig. 4. The nanoparticles obtained by laser irradiation in MO-PEG aqueous solution were like those

prepared from raw materials and pure water, with aggregates of spherical particles, 0.003 vol%: 39 ± 8 nm, 0.006 vol%: 41 ± 8 nm, and 0.012 vol%: 38 ± 9 nm (Fig. 3 (a-c), Fig. 4 (a-c)). Comparing the primary particle size with that of the raw material shown in Fig. 1 (a), the nanoparticles obtained from the raw material and in aqueous MO-PEG solution were almost equal in size, indicating that fragmentation of the raw material did not occur in laser irradiation of carbon black suspension in MO-PEG solution as well as in pure water. It became clear that no fragmentation of the raw material occurred.

In a previous study, irradiation of approximately 50 nm nanocarbon material with a vertical unfocused laser (wavelength of 532 nm, repetition rate of 30 Hz, pulse width of 8 ns) at a fluence of approximately 0.4 J/cm^2 for 30 minutes did not cause fragmentation and produced core-shell structures [47]. This is considered to be carbon onions and hollow carbon nanoparticles produced by laser annealing to carbon black, which are considered to be precursors in the fabrication of carbon nanoparticles by PLAL [48, 49]. Recently, it has been reported that fragmentation of carbon nanoparticles of about 100 nm to 5 nm was achieved by irradiating a horizontal unfocused laser (wavelength 532 nm, repetition rate 10 Hz, pulse width 10 ns) with a fluence of about 0.26 J/cm^2 for 3 hours [50]. The primary particle size of the raw material used in this study was about 33 nm and the laser fluence was up to 0.6 J/cm^2, which may indicate that the size and fluence of the raw material were sufficient for fragmentation to occur. Therefore, it is inferred that the primary particle size reduction did not occur because the light and heat energy supplied by the laser was consumed or diffused into the solvent by the sublimation and graphitization of carbon atoms inside the carbon black and the melting of carbon black particles by the short laser exposure time [48].

DLS measurements of nanoparticles obtained by laser irradiation of carbon black suspensions in pure water and in aqueous MO-PEG solutions are shown in Fig. 5. (Fig. 5 (a)). On the other hand, nanoparticles produced at different MO-PEG concentrations with a laser fluence of 600 mJ/cm^2 showed a nearly constant secondary particle diameter of about 100 nm (Fig. 5 (b)). In all results, the secondary particle diameter is smaller than that of the raw material (about 4 um).

SEM was observed and measured in solid and DLS in liquid, the agreement between SEM and DLS particle diameters indicates that the particles are dispersed in the solvent nanoparticles prepared in this study was approximately

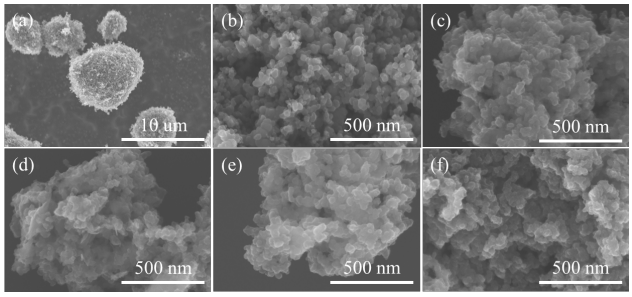

Fig. 1 (a, b) SEM images of raw material, (c-f) CNPs obtained by laser ablation in pure water. Fluence: (c) 75 mJ/cm^2, (d) 150 mJ/cm^2, (e) 300 mJ/cm^2, (f) 600 mJ/cm^2.

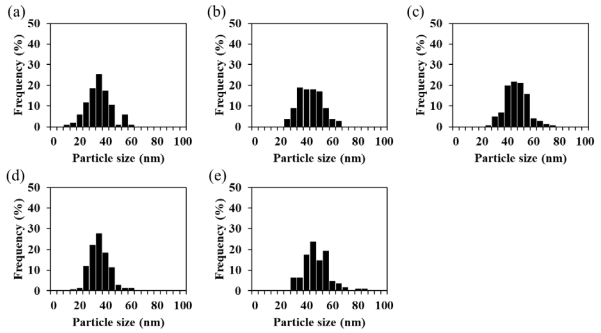

Fig. 2 (a) Size distribution of raw material (b-e) nanoparticles obtained by laser ablation in pure water. Fluence: (b) 75 mJ/cm^2, (c) 150 mJ/cm^2, (d) 300 mJ/cm^2, (e) 600 mJ/cm^2.

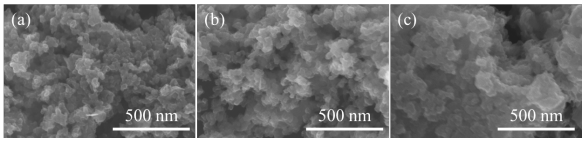

Fig. 3 SEM images of nanoparticles by laser ablation in MO-PEG solution. Concentration of MO-PEG: (a) 0.003 vol%, (b) 0.006 vol%, (c) 0.012 vol%.

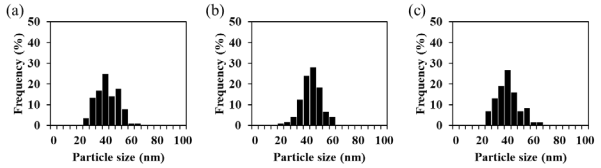

Fig. 4 Size distribution of nanoparticles obtained by laser ablation in MO-PEG solutions. Concentration of MO-PEG: (a) 0.003 vol%, (b) 0.006 vol%, (c) 0.012 vol%.

twice that of the primary particle size, suggesting that the CNPs exist in aggregation in the solvent, although they are progressively finer from micron order to nanometer order. This may be due to the small primary particle size of the raw material, as in the SEM results, and the fact that the heat and light energy supplied by the laser was consumed by the sublimation and melting of the carbon atoms, or by diffusion from the particle surface into the solvent. The particle size of the prepared CNPs was also found to meet the guideline of 10 nm to 200 nm for medical applications, as they are easily absorbed by cancer cells and are not excreted out of the body through the kidney or liver.

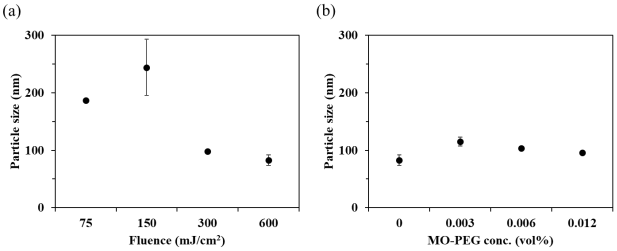

Fig. 5 DLS measurements of nanoparticles obtained by pulsed laser ablation in liquid in (a) pure water (b) MO-PEG.

The UV-Vis spectra of nanoparticles obtained by laser irradiation of carbon black suspensions in pure water and in

aqueous MO-PEG solutions are shown in Fig. 6. All nanoparticles obtained a peak at 260 nm assigned to the π-π* transition derived from the C=C bond in the graphite structure [51]. In addition, at 150, 300, and 600 mJ/cm^2, polyynes, a compound with triple conjugated bonds of carbon (Fig. 6 (b-d)), a by-product of laser ablation of carbon materials, were observed at 215 nm [52, 53], and at 600 mJ/cm^2, a peak at 340 nm assigned to a carbonyl group (C=O) derived n-π* transition peak at 340 nm (Fig. 6 (d, e))[54]. Furthermore, the absorbance tended to increase with increasing MO-PEG concentration, suggesting that many nanoparticles were dispersed and present in the solvent, and that the introduction of MO-PEG increased the yield of nanoparticles due to the greater effect of steric hindrance [55, 56].

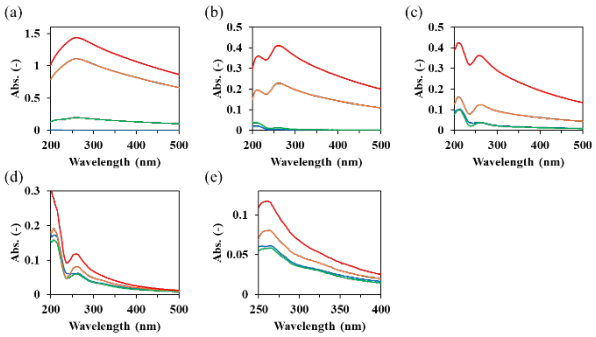

Fig. 6 (a-e) UV-Vis spectra at each fluence and concentration. Fluence: (a) 75 mJ/cm^2, (b) 150 mJ/cm^2, (c) 300 mJ/cm^2, (d) 600 mJ/cm^2 (e) Expanded spectra of (d). Concentration of MO-PEG: (blue) pure water, (green) 0.003 vol%, (yellow) 0.006 vol%, (red) 0.012 vol%.

A plot of the relationship between ablation threshold and raw material particle size for the causes of the change in UV-Vis spectral shape with different laser fluences is shown in Fig. 7. The spectra are based on the heating, melting, and evaporation model reported by Koshizaki et al. [57]. They worked to simplify the model previously reported by Pyatenko et al. and expressed the laser fluence required to melt the material with the following equation, assuming no heat loss during the conversion from optical energy to thermal energy and no heat loss to the surroundings during the increase in particle temperature [57, 58].

$$J = \frac{2}{3}\rho_p \Delta\tilde{H}\frac{d}{Q^{\lambda}_{abs}(d)} \quad , \qquad (1)$$

where J is the laser fluence of a single pulse, d is the diameter of the particle, ρ_p is the density of the particle, $Q^{\lambda}_{abs}(d)$ is the dimensionless absorption efficiency (absorption cross section/geometric cross section), and ΔH is the enthalpy required from room temperature to melting point. To determine the fluence required to melt a substance, the refractive index, enthalpy, and dimensionless absorption efficiency of the substance are necessary. For the refractive index and enthalpy, previously published values were used [59, 60], and the dimensionless effective absorption cross section was obtained by Mie calculations, which were calculated in the present study by using software [61], All calculations were performed assuming monodisperse carbon black in water. Furthermore, since graphite sublimates at high temperatures without melting, this plot shows the fluence required for carbon black to sublimate, with the upper portion being gas and the lower portion solid relative to the line connecting the plots with a straight line [61, 62]. The plots produced indicate that as the particle size of the raw material increases, a higher fluence is required for ablation. From the results in Fig. 7, it can be inferred that the minimum ablation threshold is 137 mJ/cm^2 (particle size 100 nm) and that the fused carbon black particles underwent evaporation, photochemical reactions and plasmaisation with laser irradiation above the threshold value, resulting in the appearance of peaks in the spectrum above 150 mJ/cm^2, it is inferred that polyynes at 215 nm and n-π* transition peaks at 340 nm at 600 mJ/cm^2, which were not seen at 75 mJ/cm^2 [53, 62].

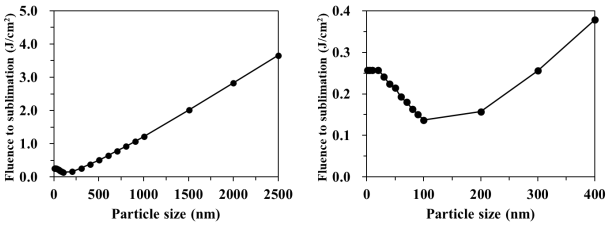

Fig. 7 (a) Relationship between particle size and ablation threshold value, (b) expanded spectra of (a).

Fig. 8 (a) shows the fluorescence spectra of nanoparticles obtained by laser irradiation of carbon black suspension in pure water and MO-PEG solution at a laser fluence of 600 mJ/cm^2, and Fig. 8 (b) shows the peak intensity ratio of the 540 nm and 460 nm of each fluorescence spectrum. Fig.8 (b) shows the results of the ratio of the peak intensities at 540 nm and 460 nm for each of the fluorescence spectra. All nanoparticles yielded peaks at 540 nm and 460 nm, indicating that they have dual blue and green emission properties (Fig. 8 (a)). The peak intensity ratio of 540 nm/460 nm depended on the MO-PEG concentration, indicating that blue fluorescence tended to be stronger than green fluorescence at higher MO-PEG concentrations, suggesting that the surfactant MO-PEG affected the optical properties of the nanoparticles (Fig. 8 (b)). Yildiz et al. used MO-PEG to study the emulsification and water solubilization of curcumin, which has low water solubility, and found that curcumin aggregated in MO-PEG aqueous solution, whereas when acetic acid solution was used instead of water, a stable emulsion was formed and curcumin was dispersed, for the nanoparticles produced in this study, the dispersion of the particles is also expected to be enhanced in an acidic environment [63]. Cancer cells are generated by a combination of poor vascular perfusion and local hypoxia, and energy metabolism is carried out by the transcription factor HIF-1α for the purpose of proliferation and tissue expansion. During this process, a large amount of glucose is consumed to produce lactic acid, and while the pH of normal tissues is approximately 7.5 [64], the pH of cancer cells is known to be acidic, ranging from 6.0-6.5 [65]. Furthermore, Shen et al. demonstrated that P-gp, a cell membrane glycoprotein known to be an obstacle to drug therapy because it lowers intracellular drug concentrations, is inhibited by polyethylene glycol derivatives, suggesting that MO-PEG can provide highly efficient cancer cell imaging [66]. Therefore, the present results can realize “highly accurate & highly efficient” cancer cell imaging using the difference in pH between cancer cells and normal cells [67, 68, 69].

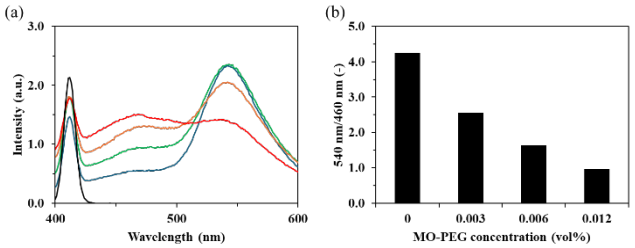

Fig. 8 PL spectra of nanoparticles obtained at fluence 600 mJ/cm^2. (black) Only pure water without nanoparticle. Concentration of MO-PEG: (blue) 0.000 vol%, (green) 0.003 vol%, (yellow) 0.006 vol%, (red) 0.012 vol%. (b) Relationship between peak intensity ratio at 540 nm and 460 nm and MO-PEG concentration.

To determine the cause of the double emission in the fluorescence spectrum of Fig. 8, Raman spectra were measured. The results are shown in Fig. 9 (a), and the peak intensity ratio of the D band to the G band (D/G ratio) obtained from the spectrum is shown in Fig. 9 (b). The normalized spectra of the D- and G-bands, respectively, are also shown in Fig. 10. The Raman spectra shows that the raw materials and the fabricated nanoparticles exhibit a D band peak around 1340 cm^{-1} indicating a disordered structure of sp^2 carbon clusters and a G band peak around 1584 cm^{-1} corresponding to the in-plane stretching vibration mode E_{2g} of single crystal graphite [70] (Fig.9 (a)). and G band intensity ratio (D/G ratio) represents the ratio of crystallinity and sp^3/sp^2 carbon [24]. The D/G ratio of the raw material was 1.68. After laser irradiation, the product decreased to 0.000 vol%: 1.19, 0.003 vol%: 0.81, 0.006 vol%: 0.63, and 0.012 vol%: 0.33 (Fig. 9 (b)). This is presumably due to the capping of MO-PEG molecules on the surface of the graphitized nanoparticles by laser irradiation, which suppressed the melting of the particles by laser irradiation and their amorphization by cooling, thereby increasing the sp^2 carbon content [71]. While the G-band peak of the raw material was at 1584 cm^{-1}, the fabricated nanoparticles had a peak at 1565 cm^{-1}, indicating a negative shift in the G-band (Fig. 10). From the resonance theory of π-electrons and polarization rates, they found that the negative shift in the G-band originates from the phase transition from graphite to amorphous carbon [70]. Since there was also a change in the D/G ratio of the raw material and the fabricated nanoparticles, it is assumed that the distortion and structural defects in the sp^2 carbon in carbon black caused by the laser irradiation were also responsible

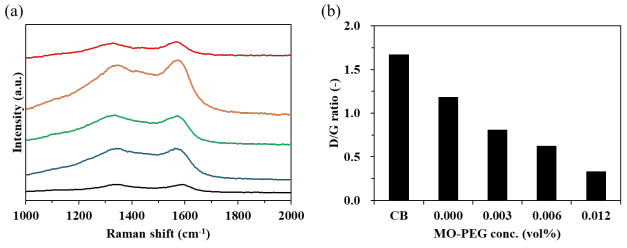

Fig. 9 (a) Raman spectra of nanoparticles obtained at fluence 600 mJ/cm^2. (black) Raw material. Concentration of MO-PEG: (blue) 0.000 vol%, (green) 0.003 vol%, (yellow) 0.006 vol%, (red) 0.012 vol%. (b) Peak intensity ratio of G-band (1600 cm^{-1}) and D-band (1350 cm^{-1}) at each concentration.

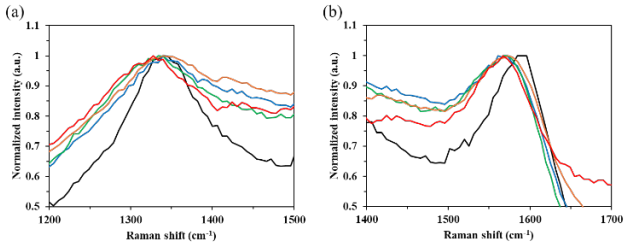

Fig. 10 Expanded Raman spectra of nanoparticles obtained at 600 mJ/cm^2. (a) G-band (1600cm^{-1}), (b) D-band (1350 cm^{-1}). Concentration of MO-PEG: (blue) 0.000 vol%, (green) 0.003 vol%, (yellow) 0.006 vol%, (red) 0.012 vol%.

for the present peak shift [70, 72].

To identify the various functional groups, present on the surface of the fabricated nanoparticles, FT-IR spectra were measured, and the results are shown in Fig. 11. The prepared nanoparticles exhibited C-O stretching vibration at 1000-1040 cm^{-1}, C-O-C asymmetric stretching vibration at 1090 cm^{-1}, C-OH stretching vibration at 1190 cm^{-1}, C-H stretching vibration at 1350, 1456, 1590 cm^{-1}, C=O stretching vibration at 1740 cm^{-1}, C-H stretching vibration at 2910-2920 cm^{-1}, and OH stretching vibration peaks at 3000-3670 cm^{-1} [50, 73, 74, 75]. For the peaks of C=O stretching vibration and C-O-C asymmetric stretching vibration, there is a difference in the IR spectra between nanoparticles fabricated in pure water and those fabricated in MO-PEG solution. The difference in these peaks indicates that MO-PEG was introduced into the nanoparticles.

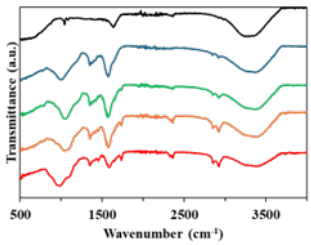

Fig. 11 IR spectra of nanoparticles obtained at 600 mJ/cm^2. (black) Raw material. Concentration of MO-PEG: (blue) 0.000 vol%, (green) 0.003 vol%, (yellow) 0.006 vol%, (red) 0.012 vol%.

From the normalized Raman spectrum shown in Fig. 10, the G band at 1584 cm^{-1} shows a peak shift between the raw material and the product obtained by laser irradiation, confirming the distortion of the sp^2 carbon. The IR spectrum shown in Fig. 11 also shows C-O stretching vibration and C-O-C asymmetric stretching vibration, and these peaks are not seen in the raw material, suggesting that they were formed by laser irradiation. From the Raman spectra and IR spectra, it is inferred that the carbon nanoparticles contained C-O-C and C-OH, and ab initio calculations by Yan et al. indicate that the epoxide (C-O-C) and hydroxyl (C-OH) of the sp^2 carbon form another energy level in the n-π* gap. It has been shown that they can do so [76]. Zhang et al. investigated the effect of C-O-C and C-OH in carbon nanoparticles on optical properties and found that the content of C-O-C and C-OH was related to the broadening of the PL peak, or multicolor emission of carbon nanoparticles [77].

Subsequent studies showed that carbon nanoparticles with excellent dispersibility have a PL peak at 450 nm, and the PL peak shifts to 550 nm as the nanoparticle concentration increases. Based on this result, a model was proposed in which carbon nanoparticle aggregates reabsorb the blue light emitted by monodisperse carbon nanoparticles and emit yellow light [78]. Therefore, in the PL spectrum of Fig. 8, for the sample with a MO-PEG concentration of 0.000 vol% with no surfactant added, green fluorescence was seen because the carbon nanoparticle aggregates containing C-O-C and C-OH were abundant and blue fluorescence was absorbed. For the sample with MO-PEG, it is considered that increasing the MO-PEG concentration increased the effect of steric hindrance of MO-PEG molecules, resulting in the formation of more monodisperse nanoparticles and a decrease in the composition ratio of aggregates. Therefore, in addition to the formation of epoxide and hydroxy groups on the sp^2 carbon of carbon black by laser irradiation, the formation of monodisperse carbon nanoparticles due to steric hindrance of surfactants can be inferred as the cause of the nanoparticles with different optical properties obtained with increasing MO-PEG concentration.

4. Conclusion

Carbon nanoparticles were successfully prepared by pulsed laser ablation in liquid in pure water and a nonionic surfactant solution. Spherical particles were obtained because of laser irradiation of carbon black suspended in an aqueous solution of polyethylene glycol monooleate, and the secondary particle size was reduced compared to the raw material, with the primary particle size being approximately 40 nm, which is almost constant. The secondary particle size was about 100 nm, indicating that CNPs existed agglomerated in the solvent and were suitable for biomedical applications; as the MO-PEG concentration increased, the amounts of nanoparticles in the dispersion increased and the absorbance increased. The prepared CNPs had peaks at 540 nm and 460 nm, and the ratio of peak intensities at 540 nm and 460 nm tended to decrease with increasing MO-PEG concentration. The intensity ratio of the D- to G-band of the raw material was 1.68, whereas it increased to 0.33-1.19 for the product after laser irradiation, and a negative peak shift of the G band occurred. MO-PEG-derived peaks such as C=O stretching vibrations and C-O-C asymmetric stretching vibrations were also observed. This may be due to laser irradiation-induced crystallization of carbon black particles (graphitization) and structural defects in the sp^2 carbon. To the best of our knowledge, this is the first successful preparation of dual fluorescent carbon nanoparticles by pulsed laser ablation in liquid under controlled surfactant concentration, and the prepared carbon nanoparticles are useful for biomedical applications including bioimaging.

Acknowledgements

The authors would like to thank Prof. Yoshitaka Kitamoto for SEM and DLS at Institute of Science Tokyo. Materials Analysis Division, Open Facility Center, Tokyo Tech supported this study.

References

[1] W.C.W Chan, D.J. Maxwell, X. Gao, R.B. Bailey, M. Han, and S. Nie: Curr. Opin. Biotechnol., 13, (2002) 40.
[2] M. Han, X. Gao, J.Z. Su, and S. Nie: Nat. Biotechnol., 19, (2001) 631.
[3] D. Gerion, F. Pinaud, S.C. Williams, W.J. Parak, D. Zanchet, S. Weiss, and A.P. Alivisatos: J. Phys. Chem. B, 105, (2001) 8861.
[4] W. Chen, A.G. Joly, and D.E. McCready: J. Chem. Phys., 122, (2005) 224708.
[5] S.-C. Pu, M.-J. Yang, C.-C. Hsu, C.-W. Lai, C.-C. Hsieh, S.H. Lin, Y.-M. Cheng, and P.-T. Chou: Small, 2, (2006) 1308.
[6] O. I. Micic, H.M. Cheong, H. Fu, A. Zunger, J.R. Sprague, A. Mascarenhas, and A.J. Nozik: J. Phys. Chem., 101, (1997) 4904.
[7] M. C. Henson and P.J. Chedrese: Exp. Biol. Med. (Maywood), 229, (2004) 383.
[8] T.H.-M. Fan, S.J. Teh, D.E. Hinton, and R.M. Higashi: Aquat Toxicol., 57, (2002) 65.
[9] J. Geys, A. Nemmar, E. Verbeken, E. Smolders, M. Ratoi, M.F. Hoylaerts, B. Nemery, and P.H.M. Hoet: Environ. Health Perspect., 116, (2008) 1607.
[10] V. Ivashchenko: J. Geochem. Explor., 240, (2022) 107046.
[11] L. Grandell and M. Hook: Sustainability, 7, (2015) 11818.
[12] X. Xu, R. Ray, Y. Gu, H.J. Ploehn, L. Gearheart, K. Raker, and W.A. Scrivens: J. Am. Chem. Soc., 126, (2004) 12736.
[13] Y. Guo, Z. Wang, H. Shao, and X. Jiang: Carbon, 52, (2013) 583.
[14] G.A. Posthuma-Trumpie, J.H. Wichers, M. Koets, L.B.J.M. Berendsen, and A. van Amerongen: Anal. Bioanal. Chem., 402, (2012) 593.
[15] H. Li, R. Liu, S. Lian, Y. Liu, H. Huang, and Z. Kang: Nanoscale, 5, (2013) 3289.
[16] H. Li, R. Liu, Y. Liu, H. Huang, H. Yu, H. Ming, S. Lian, S.-T. Lee, and Z. Kang: J. Mater. Chem., 22, (2012) 17470.
[17] V.B. Kumar, S.K. Mirsky, N.T. Shaked, and E. Gazit: ACS Nano, 18, (2024) 2421.
[18] S. Yalshetti, B. Thokchom, S.M. Bhavi, S.R. Singh, S.R. Patil, B.P. Harini, M. Sillanpaa, J.G. Manjunatha, B.S. Srinath, and R.B. Yarajarla: Sci. Rep., 14, (2024) 9915.
[19] J.V. Kumar and J.-W. Rhim, J. Environ. Chem. Eng., 12, (2024) 111999.
[20] S.-T. Yang, L. Cao, P.G. Luo, F. Lu, X. Wang, H. Wang, M.J. Meziani, Y. Liu, G. Qi, and Y.-P. Sun: J. Am. Chem. Soc., 131, (2009) 11308.
[21] X. Huang, F. Zhang, L. Zhu, K.Y. Choi, N. Guo, J. Guo, K. Tackett, P. Anilkumar, G. Liu, Q. Quan, H.S. Choi, G. Niu, Y.-P. Sun, S. Lee, and X. Chen: ACS Nano, 7, (2013) 5684.
[22] H. Zhu, X. Wang, Y. Li, Z. Wang, F. Yang, and X. Yang: Chem. Commun., 34, (2009) 5118.
[23] A.B. Bourlinos, A. Stassinopoulos, D. Anglos, R. Zboril, M. Karakassides, and E.P. Giannelis: Small, 4, (2008) 455.
[24] Z.-C. Yang, X. Li, and J. Wang: Carbon, 49, (2011) 5207.
[25] S. Sahu, B. Behera, T.K. Maiti, and S. Mohapatra: Chem. Commun., 48, (2012) 8835.
[26] J. Wang, C.-F. Wang, and S. Chen: Angew. Chem. Int. Ed., 51, (2012) 9297.

[27] H. Liu, T. Ye, and C. Mao: Angew. Chem. Int. Ed., 46, (2007) 6473.
[28] J. Zhou, C. Booker, R. Li, X. Zhou, T.-K. Sham, X. Sun, and Z. Ding: J. Am. Chem. Soc., 129, (2007) 744.
[29] S.B. Ogale, P.P. Patil, D.M. Phase, Y.V. Bhandarkar, S.K. Kulkarni, S. Kulkarni, S.V. Ghaisas, S.M. Kanetkar, V.G. Bhide, and S. Guha: Phys. Rev. B., 36, (1987) 8237.
[30] P.P. Patil, D.M. Phase, S.A. Kulkarni, S.V. Ghaisas, S.K. Kulkarni, S.M. Kanetkar, S.B. Ogale, and V.G. Bhide: Phys. Rev. Lett., 58, (1987) 238.
[31] E. Fazio, B. Gokce, A. De Giacomo, M. Meneghetti, G. Compagnini, M. Tommasini, F. Waag, A. Lucotti et al.: Nanomaterials, 10, (2020) 2317.
[32] J. Xiao, P. Liu, and C.X. Wang: Prog. Mater. Sci., 87, (2017) 140.
[33] N.G. Semaltianos: Crit. Rev. Solid State Mater. Sci., 35, (2010) 105.
[34] Y. Onodera, T. Nunokawa, O. Odawara, and H. Wada: J. Lumin., 137, (2013) 220.
[35] G.-W. Yang, J.-B. Wang, and Q.-X. Liu: J. Phys.: Condens. Matter, 10, (1998) 7923.
[36] S.R.M. Santiago, T.N. Lin, C.T. Yuan, J.L. Shen, H.Y. Huang, and C.A.J. Lin: Phys. Chem. Chem. Phys., 18, (2016) 22599.
[37] S. Hu, J. Liu, J. Yang, Y. Wang, and S. Cao: J. Nanopart. Res., 13, (2011) 7247.
[38] S. Hu, Y. Dong, J. Yang, J. Liu, and S. Cao: J. Mater. Chem., 22, (2012) 1957.
[39] Drug Evaluation and Control Division: "Pharmaceuticals and Consumer Health Bureau, Japanese Pharmaceutical Excipients" ed by Ministry of Health and Welfare, (Publisher, Japan, 2018) p.772.
[40] Y. Matsumura and H. Maeda, Cancer Res., 46, (1986) 6387.
[41] S.M.A. Sadat, S.T. Jahan, and A. Haddadi, J. Biomater. Nanobiotechnol., 7, (2016) 91.
[42] M. Yokohama, Drug. Delivery System, 33, (2018) 89.
[43] S.-L. Hu, K.-Y. Niu, J. Sun, J. Yang, N.-Q. Zhao, and X.-W. Du: J. Mater. Chem., 19, (2009) 484.
[44] V. Thongpool, P. Asanithi, and P. Limsuwan: Procedia Engineering, 32, (2012) 1054.
[45] V. Thongpool, A. Phunpueok, V. Piriyawong, S. Limsuwan, and P. Limsuwan, Energy Procedia, 34, (2013) 610.
[46] D. Reyes-Contreras, M. Camacho-Lopez, M.A. Camacho-Lopez, S. Camacho-Lopez, R.I. Rodriguez-Beltran, and M. Mayorga-Rojas: Opt. Laser Technol., 74, (2015) 48.
[47] X. Li, H. Wang, Y. Shimizu, A. Pyatenko, K. Kawaguchi, and N. Koshizaki: Chem. Commun., 47, (2011) 932.
[48] R.L.V Wal, A.J. Tomasek, and T.M. Ticich: Nano Lett., 3, (2003) 223.
[49] S. Hu, Y. Dong, J. Yang, J. Liu, and S. Cao: J. Mater. Chem., 22, (2012) 1957.
[50] F.R.U. Cortes, E. Falomir, J. Lancis, and G. Minguez-Vega: Appl. Surf. Sci., 665, (2024) 160326.
[51] V. Nguyen, L. Yan, J. Si, and X. Hou: J. Appl. Phys., 117, (2015) 084304.
[52] G. Compagnini, P. Russo, F. Tomarchio, P. Puglisi, L.D. Urso, and S. Scalese: Nanotechnology, 23, (2012) 505601.
[53] M. Tsuji, T. Tsuji, S. Kuboyama. S.-H. Yoon, Y. Korai, T. Tsujimoto, K. Kubo, A. Mori, and I. Mochida: Chem. Phys. Lett, 355, (2002) 101.
[54] I.C. Novoa-De Leon, J. Johny, S. Vazquez-Rodriguez, N. Garcia-Gomez, S. Carranza-Bernal, I. Mendivil, S. Shaji, and S. Sepulveda-Guzman: Carbon, 150, (2019) 455.
[55] N.V. Tarasenko, A.V. Butsen, and E.A. Nevar: Appl. Surf. Sci., 247, (2005) 418.
[56] C.R. Moura, R.S.F. Pereira, M. Andritschky, A.L.B. Lopes, J. Paulo de Freitas Grilo, R. Maribondo do Nascimento, and F.S. Silva: Optics & Laser Technology, 97, (2017) 20.
[57] Y. Ishikawa, T. Tsuji, S. Sasaki, and N. Koshizaki: Prog. Mater. Sci., 131, (2023) 101004.
[58] A. Pyatenko, H. Wang, N. Koshizaki, and T. Tsuji: Laser Photonics Rev., 7, (2013) 596.
[59] B. Aleksandra and E.H. Li: J. Appl. Phys., 85, (1999) 7404.
[60] NIMS, carbon, https://www.nims.go.jp/emc/ecoinfo2/pages/C/C_md.html, 2024 (accessed 11 August 2024).
[61] Faculty of Physics. ITMO University, Mie calculator, https://physics.itmo.ru/en/mie#/spectrum, 2024 (accessed 11 August 2024).
[62] C. Donate-Buendia, R. Torres-Mendieta, A. Pyatenko, E. Falomir, M. Fernandez-Alonso, and G. Minguez-Vega: ACS Omega, 3, (2018) 2735.
[63] G. Yildiz, Z. Aydogmus, F. Senkal, and G. Turan: Food Analytical Methods, 12, (2019) 2129.
[64] I.F. Tnnock and D. Rotin: Cancer Res, 49, (1989) 4373.
[65] A. Anemome, L. Consolino, F. Arena, M. Capozza, and D.L. Longo: Cancer Metastasis Rev., 38, (2019) 25.
[66] Q. Shen, Y. Lin, M. Doi, M. Sugie, K. Wakayama, N. Okada, T. Fujita, and A. Yamamoto: Int. J. Pharm, 313, (2006) 49.
[67] P. Zhao, K. He, Z. Zhang, M. Yu, H. Wang, Y. Huang, Z. Nie, and S. Yao: Anal. Chem., 87, (2015) 9998.
[68] L. Wu, Q.-S. Guo, and Q.-J. Sun: Anal. Chem., 87, (2015) 5318.
[69] P. Wu, C. Xu, X. Hou, J.-J. Xu, and H.-Y. Chen: Chem. Sci., 6, (2015) 4445.
[70] A.C. Ferrari and J. Robertson: Phys. Rev. B, 61, (2000) 14095.
[71] H. Li, Z. Kang, Y. Liu, and S.-T. Lee: J. Mater. Chem., 22, (2012) 24230.
[72] A.C. Ferrari, J.C. Meyer, V. Scardaci, C. Casiraghi, M. Lazzeri, F. Mauri, S. Piscanec, D. Liang, K.S. Noboselov, S. Roth, and A.K. Geim: Phys. Rev. Lett, 97, (2006) 187401.
[73] J. S. Anjali Devi, A.H. Anulekshmi, S. Salini, R.S. Aparna, and S. George: Microchimica Acta, 184, (2017) 4081.
[74] A. Singh, P.K. Mohapatra, D. Kalyanasundaram, and S. Kumar: Mater. Chem. Phys., 225, (2019) 23.
[75] F. Zhang, X. Feng, Y. Zhang, L. Yan, Y. Yang, and X. Liu: Nanoscale, 8, (2016) 8618.
[76] J.-A. Yan, L. Xian, and M.Y. Chou: Phys. Rev. Lett, 103, (2009) 086802.
[77] Y. Zhang, Y. Hu, J. Lin, Y. Fan, Y. Li, Y. Lv, and X. Liu: ACS Appl. Mater. Interfaces, 8, (2016) 25454.

[78] Y. Zhang, P. Zhuo, H. Yin, Y. Fan, J. Zhang, X. Liu, and Z. Chen: ACS Appl. Mater. Interfaces, 11, (2019) 24395.

(Received: November 18, 2024, Accepted: March 24, 2025)